Energy Versus Angular Momentum in Black Hole Binaries

Thibault Damour,[1] Alessandro Nagar,[1] Denis Pollney,[2] and Christian Reisswig[3]

[1]*Institut des Hautes Etudes Scientifiques, 91440 Bures-sur-Yvette, France*

[2]*Departament de Fisica, Universitat de les Illes Balears, Palma de Mallorca, E-07122, Spain*

[3]*Theoretical Astrophysics Including Relativity, California Institute of Technology, Pasadena, California 91125, USA*

(Received 13 October 2011; published 28 March 2012)

Using accurate numerical-relativity simulations of (nonspinning) black-hole binaries with mass ratios 1:1, 2:1, and 3:1, we compute the gauge-invariant relation between the (reduced) binding energy E and the (reduced) angular momentum j of the system. We show that the relation $E(j)$ is an accurate diagnostic of the dynamics of a black-hole binary in a highly relativistic regime. By comparing the numerical-relativity $E^{\rm NR}(j)$ curve with the predictions of several analytic approximation schemes, we find that, while the canonically defined, nonresummed post-Newtonian–expanded $E^{\rm PN}(j)$ relation exhibits large and growing deviations from $E^{\rm NR}(j)$, the prediction of the effective one body formalism, based purely on known analytical results (without any calibration to numerical relativity), agrees strikingly well with the numerical-relativity results.

DOI: 10.1103/PhysRevLett.108.131101 PACS numbers: 04.30.Db, 04.25.Nx, 95.30.Sf

Introduction.—A ground-based network of interferometric gravitational wave (GW) detectors is currently being upgraded and is expected, thanks to an improved sensitivity, to detect, within a few years, the GW signals emitted during the inspiral and merger of compact binaries. The realization of this exciting observational prospect depends, however, on our theoretical ability to accurately compute, within Einstein's theory of general relativity, the motion of compact binaries and its associated GW emission. Recent developments have made it clear that the most efficient way to theoretically understand the late stages of the dynamics of compact binaries is to combine the knowledge coming from analytical relativity techniques, such as traditional post-Newtonian (PN) expansions [1–4], or the newer effective one body (EOB) formalism [5–8], with the knowledge coming from numerical-relativity (NR) simulations (see [9] for a recent review). Here, we shall restrict our attention to binaries composed of two nonspinning black holes of masses m_1 and m_2. Our technique can, however, be applied to more general systems.

The aim of this Letter is to present how NR data can be used to explore, in a quite direct manner, the *dynamics* of black-hole binaries, by computing the relation between the total energy $\mathcal{E}$ of the binary system and its total angular momentum $\mathcal{J}$. We compare the (gauge-invariant) relation $\mathcal{E}(\mathcal{J})$ extracted from NR simulations to corresponding analytical predictions from PN theory [10] and from EOB theory [7]. We show that, during the inspiral, at least up to the last stable orbit (LSO), the gauge-invariant relation $\mathcal{E}(\mathcal{J})$ is essentially independent of the current uncertainties in the analytic modeling of the emitted gravitational waveform, and can therefore inform us rather directly on the conservative dynamics of a black-hole binary. (This aspect of our work is akin to a recent study of periastron advance in black-hole binaries [11].)

Numerical relativity.—Our results are based on new, accurate numerical simulations of (nonspinning) black-hole binaries, which combine a $3+1$ Cauchy-evolved spacetime (using a variant of the "Baumgarte-Shapiro-Shibata-Nakamura-Oohara-Kojima" evolution system, with moving punctures and an extended wave zone [12,13]) with a Cauchy-characteristic extraction (CCE) technique [14,15]. The initial data for the $3+1$ evolution are conformally flat, Bowen-York Cauchy data, with the initial position and linear momenta of the punctures determined from a 3PN-accurate dynamical evolution starting from a large initial separation [16]. These initial data lead to orbits having an eccentricity $e \sim 10^{-4}$. The CCE technique yields unambiguous estimates of the waveforms at infinity, without the need to extrapolate data extracted at finite radii. Here, we consider three simulations with mass ratios $q \equiv m_2/m_1$ equal to 1, 2, and 3. The corresponding *initial* Arnowitt-Deser-Misner (ADM) total energy, $\mathcal{E}_0 \equiv \mathcal{E}_{\rm ADM}$, total angular momentum, $\mathcal{J}_0 \equiv \mathcal{J}_{\rm ADM}$ (oriented along the z axis), and (initial) eccentricity are given in Table. I.

We use these numerical simulations to compute estimates of the instantaneous values (at the retarded time t), $\mathcal{E}(t)$, $\mathcal{J}(t)$, of the system energy and angular momentum during the inspiral, by using the laws of conservation of $\mathcal{E}$ and $\mathcal{J}$ between the binary system and the emitted radiation. Namely, we compute

$$\mathcal{E}^{\rm NR}(t) = \mathcal{E}_0 - \Delta\mathcal{E}^{\rm NR}_{\rm rad}(t), \tag{1}$$

$$\mathcal{J}^{\rm NR}(t) = |\mathcal{J}_0 - \Delta\mathcal{J}^{\rm NR}_{\rm rad}(t)|, \tag{2}$$

where the radiated energy and angular momentum, between the initial (retarded) time t_0 and time t, are computed from the multipole moments $N^{\rm NR}_{\ell m}$ of the NR (complex) "news function" at infinity (we generally use units such that $G = c = 1$):

TABLE I. Properties of the initial state of the NR simulations.

q	ν	e_0	$\mathcal{E}_0^{\rm NR}$	$\mathcal{J}_0^{\rm NR}$
1	0.25	1.5×10^{-4}	0.990 519 7	0.993 256 0
2	2/9	1.2×10^{-4}	0.990 898 0	0.855 996 0
3	0.1875	7.6×10^{-4}	0.993 390 5	0.767 506 8

$$\Delta\mathcal{E}^{\rm NR}_{\rm rad}(t)=\frac{1}{16\pi}\sum_{\ell,m}^{\ell_{\rm max}}\int_{t_0}^{t}dt'|N^{\rm NR}_{\ell m}(t')|^2, \tag{3}$$

$$\Delta\mathcal{J}^{\rm NR}_{z\rm rad}(t)=\frac{1}{16\pi}\sum_{\ell,m}^{\ell_{\rm max}}\int_{t_0}^{t}dt'm\Im\{h^{\rm NR}_{\ell m}(t')[N^{\rm NR}_{\ell m}(t')]^*\}. \tag{4}$$

Here $h^{\rm NR}_{\ell m}$ is the NR multipolar metric waveform, $N_{\ell m}(t)\equiv dh_{\ell m}(t)/dt$ and $\ell_{\rm max}=8$. We do not write here the expressions for the radiative losses of the other components $\mathcal{J}_x$, $\mathcal{J}_y$ of $\mathcal{J}$. We took them into account, though they turn out to have a negligible effect on the computation of $\mathcal{J}^{\rm NR}(t)$. While $\Delta\mathcal{E}^{\rm NR}_{\rm rad}$ only depends on the news function $N(t)$ (which is a direct output of the CCE code), the angular momentum loss also depends on the metric waveform $h(t)$. We computed (for each multipole) $h(t)$ from $\Psi_4(t)=dN/dt=d^2h/dt^2$ by the frequency-domain integration procedure of [17] [with a low-frequency cutoff $\omega_0=0.032/(m_1+m_2)$]. In contrast to most studies of gravitational waveforms, we consider here the full time development of the GW emission from the start of the NR simulation; i.e., we crucially take into account the losses associated with the "junk radiation," viz. the initial burst of radiation associated to the relaxation of the unphysical Bowen-York–type initial data, before the radiation settles down to a quasistationary inspiral pattern.

Finally, we replace the two t-parametrized series $\mathcal{E}^{\rm NR}(t)$, $\mathcal{J}^{\rm NR}(t)$ by the corresponding *unparametrized* curve $\mathcal{E}^{\rm NR}(\mathcal{J})$. One example (for the mass ratio $q=1$) of our computations of the relation $\mathcal{E}(\mathcal{J})$ is shown in Fig. 1. Here and below, we work with the binding energy per reduced mass, $E\equiv(\mathcal{E}-M)/\mu$, and the dimensionless rescaled angular momentum $j\equiv\mathcal{J}/M\mu$, where $M\equiv m_1+m_2$, $\mu\equiv m_1m_2/(m_1+m_2)$. Figure 1 compares the NR relation $E^{\rm NR}(j)$ to predictions made by two different analytical formalisms: PN theory and EOB theory (as explained in detail below). The inset shows the very significant effect of the energy loss due to the junk radiation emitted at the beginning of the simulation. Note that j decreases during the inspiral.

Post-Newtonian theory.—There is a large ambiguity in using PN theory to compute any observable quantity (as illustrated for the GW phase in [18], and for the LSO in [7,19]). Here, we shall consider the *canonical* PN expansion of the (gauge-invariant) *function* $E(j)$ [10], i.e., the truncated Taylor series in powers of $1/c^2$ of $E(j,1/c^2)$. At the third post-Newtonian (3PN) level it has the structure [see Eq. (5.1) of [10]]

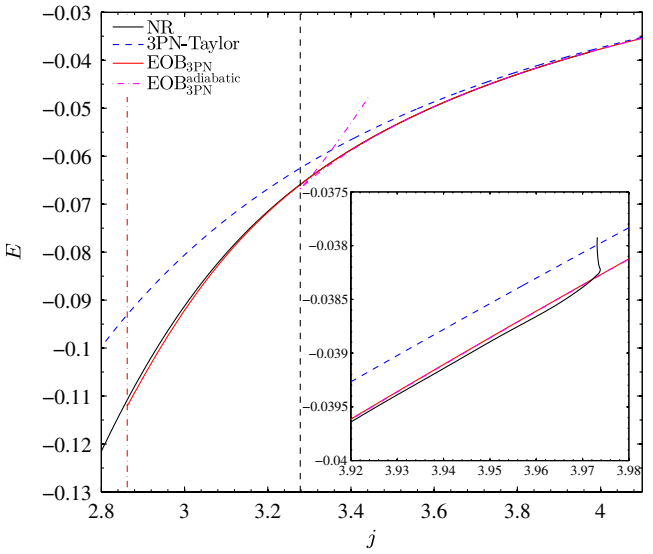

FIG. 1 (color online). Equal-mass case: comparison between four $E(j)$ curves. The Taylor PN curve shows the largest deviation from NR results, especially at low j's, while the two (adiabatic and nonadiabatic) 3PN-accurate, non–NR-calibrated EOB curves agree remarkably well with the NR one.

$$E^{\rm PN}(j)=-\frac{1}{2j^2}\left[1+\frac{c_1(\nu)}{c^2j^2}+\frac{c_2(\nu)}{c^4j^4}+\frac{c_3(\nu)}{c^6j^6}\right], \tag{5}$$

where $c_n(\nu)$ are polynomials (of order n) in the symmetric mass ratio $\nu\equiv\mu/M\equiv m_1m_2/(m_1+m_2)^2$. This canonical "Taylor" (i.e., nonresummed) $E^{\rm PN}(j)$ function is shown in Fig. 1 (for $q=1$) as a dashed line.

Effective one body theory.—The EOB formalism maps the conservative dynamics of a two-body system onto the dynamics of one body of mass μ in a stationary and spherically symmetric "effective" metric, $ds^2_{\rm eff}=-A(r;\nu)dt^2+[A(r;\nu)\bar{D}(r;\nu)]^{-1}dr^2+r^2(d\theta^2+\sin^2\theta d\varphi^2)$. The EOB potentials A and $\bar{D}$ have been computed at the 2PN approximation in [5], and at the 3PN approximation in [7] [at 3PN one must complete the geodesic dynamics by terms, $Q(p)$, quartic in momenta]. Here, we use the 3PN-accurate version of the EOB Hamiltonian, as defined in 2000 [7] (with $\omega_{\rm static}=0$ [3]), i.e., with the effective-metric potentials $\bar{D}(u)\equiv1+6\nu u^2+(52-6\nu)\nu u^3$, and $A(u)\equiv P^1_3[1-2u+2\nu u^3+(\frac{94}{3}-\frac{41}{32}\pi^2)\nu u^4]$, where $u\equiv GM/(c^2r)$, and where P^1_3 denotes constructing a (1, 3) Padé approximant, so that $A(u)$ is a rational function of u of the form $(1+n_1u)/(1+d_1u+d_2u^2+d_3u^3)$. In addition to the Hamiltonian dynamics defined by $A(u)$, $\bar{D}(u)$ [and $Q(u,p)$], the EOB formalism defines a radiation-reaction force $\mathcal{F}_\varphi$. Here, we use the "newly resummed" radiation reaction defined by [20,21], with 3^{+2}-PN accurate Taylor $\rho_{\ell m}$'s, and *without* incorporating any "next-to-quasi-circular" (NQC) correction factor. The main point is that the resulting radiation-reaction–driven EOB dynamics uses only information that has long been analytically known, and does not rely on any information deduced from comparing EOB waveforms to NR waveforms. The resulting

(nonadiabatic) 3PN-accurate, radiation-reaction driven EOB dynamics leads to the curve $E^{\mathrm{EOB}_{3\mathrm{PN}}}(j)$ shown in Fig. 1 as a solid gray (red online) line. In addition, we also show the *adiabatic* EOB $E^{\mathrm{EOB}^{\mathrm{adiabatic}}_{3\mathrm{PN}}}(j)$ curve defined by considering the sequence of minima in r (for a fixed j) of the (3PN-accurate) EOB Hamiltonian $H^{\mathrm{EOB}_{3\mathrm{PN}}}(r, j)$. This adiabatic curve *only* depends on the potential $A(u)$ and has a cusp at the LSO, j_{LSO}. [The second branch starting at the cusp corresponds to unstable circular orbits below the LSO.] The vertical distance $E^{\mathrm{EOB}_{3\mathrm{PN}}}(j) - E^{\mathrm{EOB}^{\mathrm{adiabatic}}_{3\mathrm{PN}}}(j)$ essentially represents the kinetic energy linked to the (slow) inspiralling radial motion.

Results of the triple comparison NR-PN-EOB.—Figure 1 already exhibits several of the new results of our study. (i) The NR $E(j)$ curve starts at large j's (i.e., large radial separations) close to the nonresummed PN $E(j)$ curve, but then visibly deviates more and more from it during the inspiral [conventionally ending at the adiabatic (EOB-defined) LSO, marked by a dashed vertical line]. (ii) By contrast, the NR $E(j)$ curve is so close, on the scale of Fig. 1, to the (3PN-accurate, nonadiabatic) EOB prediction that their difference is barely visible not only during the inspiral, but also during the subsequent plunge. (The leftmost vertical line in Fig. 1 denotes the EOB "light ring," viz. the end of the analytical inspiral-plus-plunge dynamics, and the beginning of the EOB description of the merger and ringdown.] (iii) On the scale of Fig. 1, one cannot see, during the inspiral, the difference between the two EOB curves (nonadiabatic versus adiabatic). (iv) In addition, when zooming on the beginning of the $E^{\mathrm{NR}}(j)$ curve (see inset), we find that, although it coincidentally starts near the PN curve, it emits exactly the amount of junk radiation required to relax to the EOB prediction. When considering the mass ratios $q = 2$ and $q = 3$, we obtained close analogs of Fig. 1, which exhibit exactly the same results (i)–(iv).

In order to refine and quantify these results, we henceforth close up on the small deviations between the various $E(j)$ curves by using, as a horizontal baseline, the (nonadiabatic, 3PN-accurate) EOB curve, i.e., by plotting the *differences* $E^X(j) - E^{\mathrm{EOB}_{3\mathrm{PN}}}(j)$, where the label X denotes either NR, PN, $\mathrm{EOB}^{3\mathrm{PN}}_{\mathrm{adiabatic}}$, or other EOB curves defined below. When focussing on the inspiral dynamics (above the LSO), this leads to NR-EOB differences of order 10^{-4}, i.e., 300 times smaller than the $\simeq 3 \times 10^{-2}$ change in the absolute value of E during the inspiral, and 50 times smaller than the PN–NR difference $\sim 5 \times 10^{-3}$ at the LSO. To discuss the meaning of the small NR-EOB differences, it is important to estimate the error attached to the NR $E^{\mathrm{NR}}(j)$ curve. We estimated an error on $E^{\mathrm{NR}}(j)$ by measuring the effect of changing, in turn, all the NR elements entering the computation of the losses given by Eqs. (3) and (4): (i) we replaced the CCE news by either the time integral of the curvature waveform $\Psi_4(t) = dN(t)/dt$ extracted at a large radius in the $3+1$ code, or a Regge-Wheeler-Zerilli metric waveform output by the latter code; (ii) we reduced the maximum multipolar order $\ell_{\max}$ used in the sums in Eqs. (3) and (4) from the default value $\ell_{\max} = 8$ to $\ell_{\max} = 7$ and $\ell_{\max} = 6$; (iii) we varied the low-frequency cutoff $M\omega_0$ used in the frequency-domain computation of $h_{\ell m}(t)$ from $\Psi_4^{\ell m}(t)$ [17] between about 0.01 and 0.04; (iv) we computed $h_{\ell m}(t)$ from $N_{\ell m}(t)$ instead of $\Psi_4^{\ell m}(t)$; (v) we explored the sensitivity to changes of the initial integration time t_0 in Eqs. (3) and (4); (vi) we replaced the high resolution NR data used as a baseline by medium resolution ones.

Adding the effect of all these changes, and focussing on the crucial change in the energy loss ΔE_{junk} linked to the initial burst of junk radiation, leads to a conservative error bar around $E^{\mathrm{NR}}(j)$ indicated by the gray-shaded region in Fig. 2. In that figure, we plot the differences $E^X(j) - E^{\mathrm{EOB}_{3\mathrm{PN}}}(j)$ for $q = 1$, 2, or 3, and for six different labels X: NR (solid, thick, black curve), PN (upper, thick dashed, blue online, curve), $\mathrm{EOB}^{\mathrm{adiabatic}}_{3\mathrm{PN}}$ (lower, dash-dotted, magenta online, curve), $\mathrm{EOB}^{\mathrm{NQC}}_{3\mathrm{PN}}$ (black, dashed curve, just below the baseline), $\mathrm{EOB}^{\mathrm{NQC}}_{5\mathrm{PN}}$ (thin, dashed gray, blue online, curve), and $\mathrm{EOB}^{\mathrm{woNQC}}_{5\mathrm{PN}}$ (upper, solid gray, blue online, curve, close to the previous one). Here, as above, the EOB

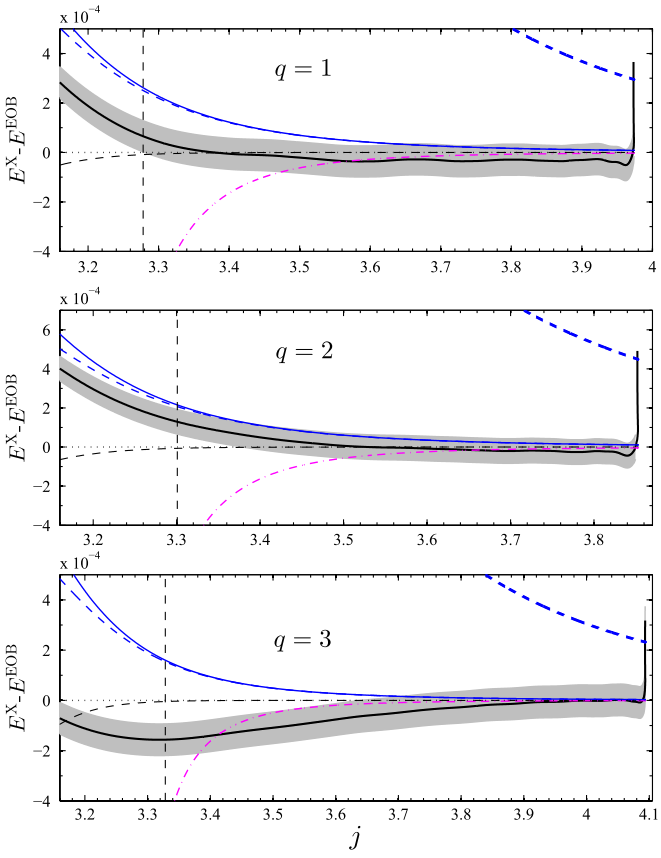

FIG. 2 (color online). Differences between seven $E^X(j)$ curves and $E^{\mathrm{EOB}_{3\mathrm{PN}}}(j)$, for the three mass ratios considered. From top to bottom the labeling is $X = \mathrm{PN}$, $\mathrm{EOB}^{\mathrm{woNQC}}_{5\mathrm{PN}}$, $\mathrm{EOB}^{\mathrm{NQC}}_{5\mathrm{PN}}$, NR, $\mathrm{EOB}_{3\mathrm{PN}}$ (baseline), $\mathrm{EOB}^{\mathrm{NQC}}_{3\mathrm{PN}}$, and $\mathrm{EOB}^{\mathrm{adiabatic}}_{3\mathrm{PN}}$. While the PN curve exhibits the largest deviations, all EOB curves remain close to the NR one during the full inspiral, especially the 3PN-accurate, *non-NR-calibrated* one.

baseline $E^{\mathrm{EOB}_{3\mathrm{PN}}}$ (corresponding to the horizontal axis), as well as its adiabatic $\mathrm{EOB}^{\mathrm{adiabatic}}_{3\mathrm{PN}}$, and NQC-completed $\mathrm{EOB}^{\mathrm{NQC}}_{3\mathrm{PN}}$ avatars, use the 3PN-accurate EOB potentials of [7]. [$\mathrm{EOB}^{\mathrm{NQC}}_{3\mathrm{PN}}$ is defined according to the methods introduced in [21] by adding a factor $f^{\mathrm{NQC}}_{22}(a_1, a_2)$ in the $\ell = m = 2$ mode, tuned to the maximum of the NR modulus.] Finally, $E^{\mathrm{EOB}^{\mathrm{NQC}}_{5\mathrm{PN}}}$ and $E^{\mathrm{EOB}^{\mathrm{woNQC}}_{5\mathrm{PN}}}$ use the NR-calibrated, 5PN potential $A_{5\mathrm{PN}}(u) = P^1_5[A^{\mathrm{Taylor}}_{3\mathrm{PN}}(u) + \nu a_5 u^5 + \nu a_6 u^6]$ for $(a_5, a_6) = (-6.3722, 50)$ [which lies in the middle of the "good region" of Ref. [21]], either with (NQC) or without (wo NQC) NQC corrections. Figure 2 allows us to refine and strengthen the conclusions drawn above from Fig. 1, namely, (i) The canonical nonresummed $E^{\mathrm{PN}}(j)$ curve disagrees strongly with the NR results; (ii) the 3PN-accurate nonadiabatic EOB curve, $E^{\mathrm{EOB}_{3\mathrm{PN}}}$ (i.e., the horizontal baseline) is remarkably close to the NR results during the entire inspiral, with deviations that are smaller than the "2σ" level; (iii) the inclusion of nonadiabatic effects is important in continuing to ensure this agreement during the late inspiral (see the difference $E^{\mathrm{EOB}^{\mathrm{adiabatic}}_{3\mathrm{PN}}} - E^{\mathrm{EOB}_{3\mathrm{PN}}}$); (iv) the inclusion of the NR-fitted NQC correction has a negligible effect during the inspiral: $E_{\mathrm{woNQC}} - E_{\mathrm{NQC}} \lesssim 2 \times 10^{-5}$; (v) the EOB predictions based on the NR-calibrated, 5PN potential $A_{5\mathrm{PN}}(u)$ of Ref. [21] (with or without NQC corrections), are slightly less close (especially for $q = 1$ and 3) to the NR result than the purely analytical 3PN-accurate EOB prediction. We verified that the same conclusion holds for the NR-calibrated 5PN EOB potential suggested in [22].

Summary.—We showed how to combine the knowledge of the initial (ADM) energy and angular momentum of a black-hole binary with accurate NR computations of its subsequent GW emission (including the initial burst of junk radiation), to derive a NR estimate of the relation between the rescaled binding energy $E \equiv (\mathcal{E} - M)/\mu$ and the rescaled angular momentum $j = \mathcal{J}/(M\mu)$. Though the relation $E^{\mathrm{NR}}(j)$ does include nonadiabatic effects (linked to the radial motion during the inspiral, and thereby to the radiation reaction $\mathcal{F}_\varphi$), we have verified that the analytic uncertainties in the description of $\mathcal{F}_\varphi$ were essentially negligible during the inspiral, down to, at least, the LSO. This potentially makes the NR-acquired knowledge of the $E(j)$ curve an accurate diagnostic of the *conservative dynamics* of a black-hole binary in a highly relativistic regime. By comparing $E^{\mathrm{NR}}(j)$ to various analytic descriptions of binary dynamics, we found that, while the canonical, nonresummed 3PN-expanded relation $E^{\mathrm{PN}}(j)$ exhibits large and growing deviations with respect to $E^{\mathrm{NR}}(j)$, the EOB formalism, based purely on known analytical results (without NR calibration), predicts a relation $E^{\mathrm{EOB}}(j)$ which is remarkably close to $E^{\mathrm{NR}}(j)$. Figure 2 clearly shows that the NR curve $E^{\mathrm{NR}}(j)$ provides us with a new, sensitive tool for exploring the dynamics of a black-hole binary. However, in order to extract from it reliable information about the conservative dynamics of the binary, one needs (as already mentioned in [21]) to take into account the fact that the energy balance between the binary system and the emitted radiation involves an extra "Schott term" [23] linked to the field energy. We leave such a study to future work.

We thank Sascha Husa for assistance in computing low eccentricity initial data. D. P. was supported by Grants No. CSD2007-00042 and No. FPA2010-16495 of the Spanish Ministry of Science. C. R. was supported by the National Science Foundation under Grants No. AST-0855535 and No. OCI-0905046. Computations were performed on the NSF Teragrid (allocations TG-MCA02N014 and TG-PHY100033), the LONI network (www.loni.org) (allocation loni_numrel05), and the Caltech computer cluster Zwicky (NSF MRI Grant No. PHY-0960291).

[1] T. Damour, Phys. Rev. Lett. **51**, 1019 (1983).
[2] L. Blanchet, T. Damour, B. R. Iyer, C. M. Will, and A. G. Wiseman, Phys. Rev. Lett. **74**, 3515 (1995).
[3] T. Damour, P. Jaranowski, and G. Schäfer, Phys. Lett. B **513**, 147 (2001).
[4] L. Blanchet, T. Damou, G. Esposito-Farèse, and B. R. Iyer, Phys. Rev. Lett. **93**, 091101 (2004).
[5] A. Buonanno and T. Damour, Phys. Rev. D **59**, 084006 (1999).
[6] A. Buonanno and T. Damour, Phys. Rev. D **62**, 064015 (2000).
[7] T. Damour, P. Jaranowski, and G. Schaefer, Phys. Rev. D **62**, 084011 (2000).
[8] T. Damour, Phys. Rev. D **64**, 124013 (2001).
[9] U. Sperhake, E. Berti, and V. Cardoso, arXiv:1107.2819.
[10] T. Damour, P. Jaranowski, and G. Schäfer, Phys. Rev. D **62**, 044024 (2000).
[11] A. Le Tiec, A. H. Mroué, L. Barack, A. Buonanno, H. P. Pfeiffer, N. Sago, and A. Taracchini, Phys. Rev. Lett. **107**, 141101 (2011).
[12] D. Pollney, C. Reisswig, N. Dorband, E. Schnetter, and P. Diener, Phys. Rev. D **80**, 121502 (2009).
[13] D. Pollney, C. Reisswig, E. Schnetter, N. Dorband, and P. Diener, Phys. Rev. D **83**, 044045 (2011).
[14] C. Reisswig N. T. Bishop, D. Pollney, and B. Szilágy, Phys. Rev. Lett. **103**, 221101 (2009).
[15] C. Reisswig, N. T. Bishop, D. Pollney, and B. Szilágy, Classical Quantum Gravity **27**, 075014 (2010).
[16] S. Husa, M. Hannam, J. A. González, U. Sperhake, and B. Brügmann, Phys. Rev. D **77**, 044037 (2008).
[17] C. Reisswig and D. Pollney, Classical Quantum Gravity **28**, 195015 (2011).
[18] T. Damour, B. R. Iyer, and B. S. Sathyaprakash, Phys. Rev. D **63**, 044023 (2001).
[19] M. Favata, Phys. Rev. D **83**, 024027 (2011).
[20] T. Damour, B. R. Iyer, and A. Nagar, Phys. Rev. D **79**, 064004 (2009).
[21] T. Damour and A. Nagar, Phys. Rev. D **79**, 081503 (2009).
[22] Y. Pan, A. Buonanno, M. Boyle, L. T. Buchman, L. E. Kidder, H. P. Pfeiffer, and M. A. Scheel, Phys. Rev. D **84**, 124052 (2011).
[23] G. A. Schott, Philos. Mag. **29**, 49 (1915).